Dielectric response of tungsten modified $Ba(Ti_{0.90}Zr_{0.10})O_3$ ceramics obtained by mixed oxide method

Francisco Moura[1], Alexandre Z. Simões[2,*], Maria A. Zaghete[3], Jose A. Varela[3], Elson Longo[3]

[1]*Universidade Federal de Itajubá- Unifei - Campus Itabira, Rua São Paulo 377, Bairro Amazonas, P.O. Box 355, 35900-37, Itabira, Minas Gerais, Brazil*

[2]*Universidade Estadual Paulista- Unesp - Faculdade de Engenharia de Campus Itabira, Av. Dr Ariberto Pereira da Cunha 333, Bairro Pedregulho, P.O. Box 355, 12.516-410, Guaratinguetá, São Paulo, Brazil*

[3]*Laboratório Interdisciplinar em Cerâmica, Instituto de Química, Universidade Estadual Paulista, P.O. Box 355, 14801-907 Araraquara, São Paulo, Brazil*

Received 4 November 2010; received in revised form 8 December 2010; accepted 16 December 2010

Abstract

The electrical response of $Ba(Ti_{0.90}Zr_{0.10})O_3$ (BZT) ceramics obtained by the mixed oxide method as a function of tungsten content was investigated. According to X-ray diffraction analysis the single phase BZT1W (1 wt.% W doped BZT) and BZT2W (2 wt.% W doped BZT) ceramics, crystallized in a perovskite structure, were obtained. It is also shown that tungsten substituted ceramics can be sintered at a reduced temperature when compared to the undoped BZT. Electron paramagnetic resonance (EPR) analyses reveals that substitution of Ti^{4+} by W^{6+} causes distortion in the crystal structure changing lattice parameter. Substitution of W^{6+} on B-site of ABO_3 perovskite BZT ceramics shifted the phase transition to lower temperatures up to a tungsten content of 2 wt.% leading to a relaxor-like behaviour.

***Keywords**: donor dopant; ceramics; dielectric response; mixed oxide method*

I. Introduction

$Ba(Ti_{1-x}Zr_x)O_3$ solid solution has received much attention due to its excellent dielectric properties for application as capacitors [1–3]. This system is attractive for dynamic random access memories and tunable microwave devices. Such, lead-free, environmentally friendly materials are known to exhibit relaxor behaviour in bulk materials with increasing Zr content. X-ray crystalline structure studies revealed that $Ba(Ti_{1-x}Zr_x)O_3$ forms a complete solid solution and the phase diagram was constructed for up to 30 at.% Zr substitution [4–6]. Most studies on $Ba(Ti_{1-x}Zr_x)O_3$ ceramics are focused on the temperature dependence of the dielectric permittivity and relaxor behaviour [7–9]. Many aliovalent compositional alterations to $Ba(Ti_{1-x}Zr_x)O_3$ have been studied either with higher valence substitutions (donors), or with lower valence ions (acceptors). Recently, it was found that the solid solubility of Y doped $BaTiO_3$ could reach up to 12.2 mol% once yttrium ions have stable valence [10]. Donor dopant,such as W^{6+}, induces cationic defects while occupying the B site of the perovskite lattice [11,12]. Such behaviour may cause several effects on the dielectric properties through interaction with domain walls [13,14]. In perovskites, the relaxor behaviour occurs mainly in lead-based compositions with more than one type of ion occupying the equivalent six coordinated crystallographic sites. Lead-free compositions can be of great interest for environmentally friendly applications such as actuators, dielectrics for capacitors, etc. Previous studies demonstrated that B-site substitution with high valent cations (Mo^{6+} and W^{6+}) enhanced the remnant polarization, P_r and reduced the coercive field, E_c [15]. In this work, we have investigated the advances in the dielectric properties of tungsten doped $Ba(Ti_{0.90}Zr_{0.10})O_3$ ceramics prepared by the mixed oxide method. Sinterability of the tungsten doped $Ba(Ti_{0.90}Zr_{0.10})O_3$ ceramics has also been investigated. Ceramics with good electrical properties were obtained confirming the possibility of use of ferroelectric perovskite materials such as barium zirconium titanate in capacitor applications.

* Corresponding author: tel: +55 12 3123 2765
fax: +55 12 3123 2800, e-mail: *alezipo@yahoo.com*

II. Experimental

$Ba(Ti_{0.90}Zr_{0.10})O_3$ (*BZT*) ceramics were prepared by solid-state reaction. $BaCO_3$ (99.997%-Vetec), TiO_2 (99.995%-Vetec) and ZrO_2 (99.978%-Inlab) starting materials with high purity were weighed and wet mixed in alcohol. After drying, the powders were calcined at 1200°C for 4 hours. Separately, tungsten oxide was dissolved in nitric acid and complexed with citric acid and ethylene glycol. The tungsten citrate solution was added to the $Ba(Ti_{0.90}Zr_{0.10})O_3$ powders and calcined at 600°C for 4 hours.

Different amounts of tungsten citrate, 0, 1.0, 2.0 and 4.0 wt.% were added to the calcined powder by wet mixing being represented by the compositions *BZT*, *BZT1W*, *BZT2W* and *BZT4W*, respectively. The powders were pressed into pellets and sintered at 1550°C for 4 hours and 1200°C for 4 hours for the *BZT* and *BZTW*, respectively. Differences in the sintering temperatures for both *BZT* and *BZTW* compositions were extracted from the shrinkage-rate-temperature curve. Pellets with the size of about 10 mm × 2 mm were obtained. The density of the sintered compacts was measured by Archimedes method.

The dilatometric analyses were performed in a Nezstch dilatometer 402E, up to 1500°C, at a heating rate of 5°C/min in static air atmosphere and the linear shrinkage rate ($d(\Delta l/l_0)/dT$) results collected at every 0.5°C. After sintering the disks were polished to 1 mm in thickness and characterized by means of electrical measurements. Gold electrodes for electrical measurements were applied by evaporation through a sputtering system in a polished surface of sintered discs. Phase formation in the *BZT* and *BZTW* ceramics was identified by X-ray diffraction using a rotate anode powder diffractometer (Rigaku Rint 2000) with CuKα radiation over the 2θ range of 20–80°. Raman measurements were performed using an ISAT 64000 triple monochromator. An optical microscope was employed to focus the 514.5-nm radiation from a Coherent Innova 99 Ar + laser on the sample and to collect the back-scattered radiation. The scattered light dispersed by the spectrometer was detected by a charge-coupled device (CCD) detection system. Microstructural characterization was performed by atomic force microscopy (AFM) using a DIGITAL, Nanoscope 3A. Electron paramagnetic resonance (EPR) spectra were recorded on a Brucker

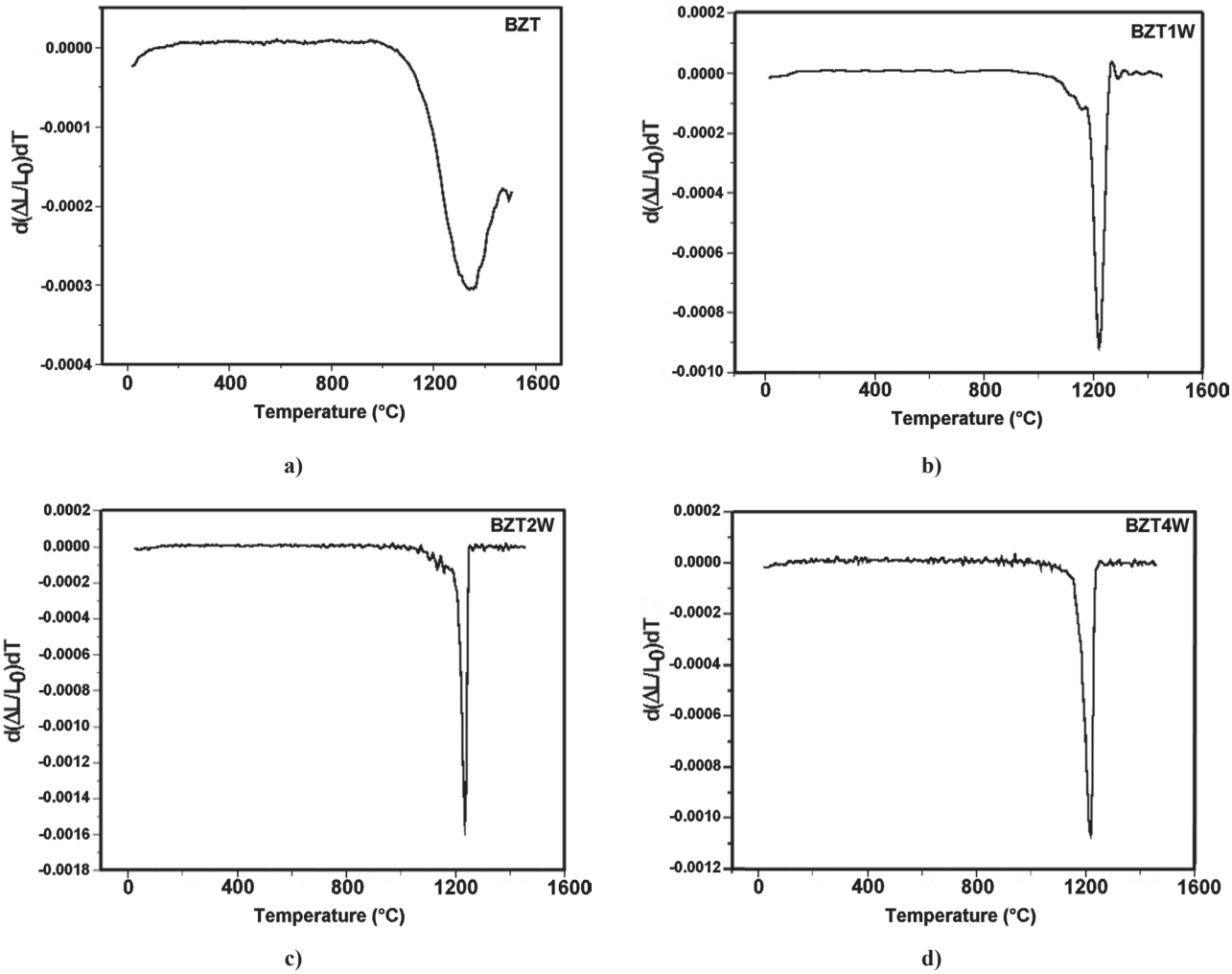

Figure 1. Linear shrinkage rate for: a) *BZT*, b) *BZT1W*, c) *BZT2W* and d) *BZT4W* ceramics prepared from mixed oxide method

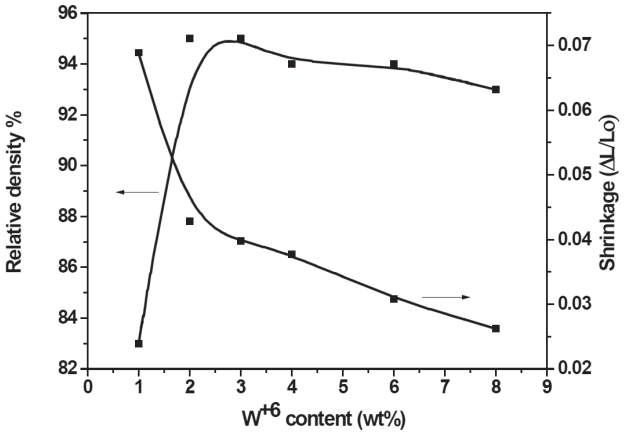

Figure 2. Dependence of density and shrinkage rate for *BZT* ceramics as a function of WO_3 content

EMX-300 Spectrometer, operating at X-band (9 GHz) and at microwave power 2 mW; amplitude modulation 1 Gauss; time constant 2.56 ms, conversion time 10.24 ms, and modulation frequency 100 kHz. The *g*-factor was referenced with respect to $MgO:Cr^{3+}$ (g = 1.9797) as the external standard. All EPR measurements were performed under room temperature (25°C) and the spectra were evaluated using the SimFonia program.

Dielectric permittivity and dielectric loss as a function of temperature and frequency were measured in a HP 4194 A LCR Meter.

III. Results and discussion

Dilatometric analyses were used to investigate the sintering process of the tungsten modified *BZT* ceramics. The linear shrinkage rate ($d(\Delta l/l_0)/dT$) as a function

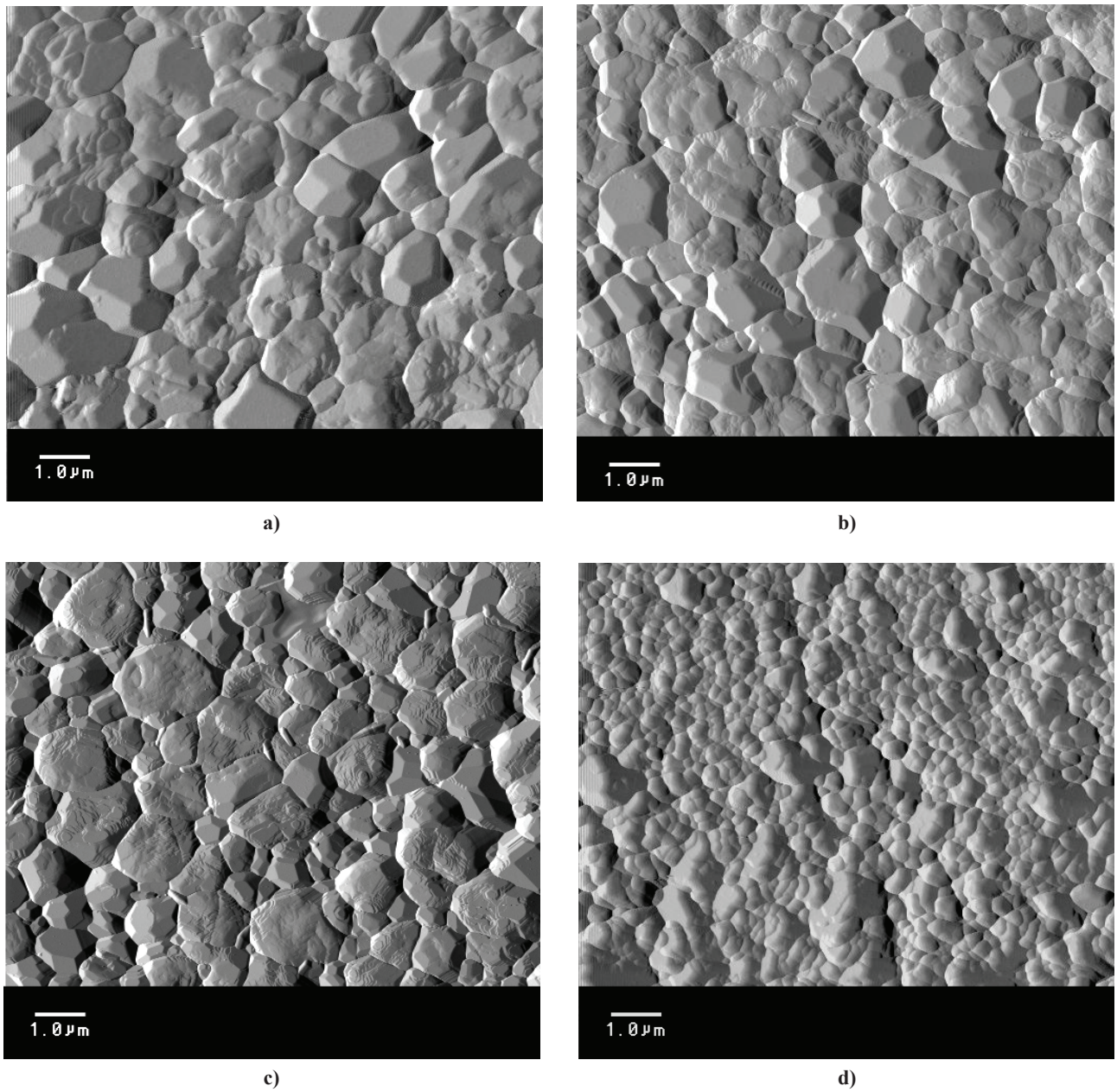

Figure 3. AFM micrographies for: a) *BZT*, b) *BZT1W*, c) *BZT2W* and d) *BZT4W* ceramics prepared from mixed oxide method

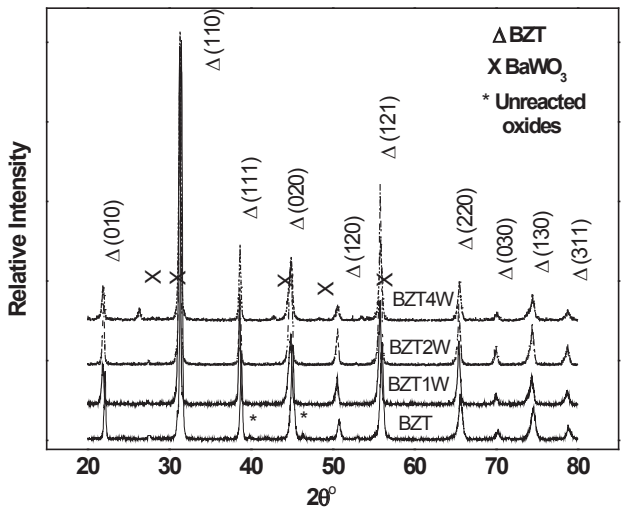

Figure 4. X-ray diffraction for *BZT*, *BZT1W*, *BZT2W* and *BZT4W* ceramics prepared from mixed oxide method

of temperature for different tungsten concentrations is shown in Fig. 1. Because of mixed oxide method being employed during preparation of the *BZTW* ceramics, hard agglomerates can be formed. To improve sinterability of these powders it was necessary to prolong milling process in order to reduce agglomerate size and activate powders for sintering. Only one maximum in the shrinkage-rate-temperature curve was registered (1200°C) and it can be attributed to a rapid elimination of the inter-particle pores. Above this temperature the shrinkage rate decreased. The densification of powders at lower temperature revealed that these agglomerates are softer. No other peaks were registered in the shrinkage-rate curve, demonstrating the presence of soft agglomerates in the calcined powders which were completely broken during milling process. As can be seen in Fig. 1, the maximum shrinkage rate occurred around 1200°C for all tungsten modified compositions and occurred around 1350°C for the undoped *BZT*. This behaviour reveals that tungsten has a strong influence on the sintering process. That can be caused by the formation of a high amount of oxygen vacancies as observed in the equations 1–8. These vacancies facilitate material diffusion during sintering.

The relative densities and shrinkage of *BZT* ceramics substituted with different WO_3 contents are illustrated in Fig 2. Final densities after sintering are close to 95% of the theoretical density. They were only slightly affected by tungsten content, although the average grain size decreased significantly. A decrease in the grain size was evident for the *BZT4W* ceramic indicating that the tungsten not only provides oxygen vacancies to facilitate the densification, but also acts as a grain growth inhibitor. It is obvious that trace amount of tungsten can greatly enhance the density of *BZT* ceramics, being the maximum value of 5.79 g/cm^3 for the *BZT2W*. The minimum density of 5.63 g/m^3 was observed for the *BZT1W* ceramic.

The microstructure of those ceramics is shown in Fig. 3. The grain growth is inhibited in the *BZT4W* sample due to the formation of $BaWO_3$ secondary phase in the grain boundary (Fig. 3c). Tungsten ion plays a role of donor in *BZT* because it possesses a higher valence than Ti or Zr suppressing the formation of oxygen vacancies. Considering that W^{+6} preferentially enter in B-sites, we expected an increase in oxygen vacancies concentration which affects the densification process. The small grain size can be interpreted by the suppression of oxygen vacancy concentration, which results in slower oxygen ion motion and consequently lower grain growth rate as it was verified in the EPR spectra. The absence of segregates in the grain boundaries of the *BZT2W* sample indicates the high solubility of WO_3 in the *BZT* matrix (Fig. 3b).

The corresponding defect reactions can be described as follows:

$$WO_3 \xrightarrow{BZT} W_{Ti}^{\bullet\bullet} + V_{Ba}^{''} + 3O_O^x \quad (1)$$

$$[MO_6]^x + [MO_5.V_o^x] \longrightarrow [MO_6]' + [MO_5.V_o^{\bullet}] \quad (2)$$

For M = Zr or Ti:

$$[V_{Ba}^{''}O_{12}] + [WO_6]^{\bullet\bullet} \longrightarrow [V_{Ba}^{x}O_{12}] + [WO_6]^x \quad (3)$$

$$[MO_5V_O^x] + [WO_6]^{\bullet\bullet} \longrightarrow [MO_5V_O^{\bullet}] + [WO_6]^{\bullet} \quad (4)$$

$$[MO_5V_O^x] + [WO_6]^{\bullet} \longrightarrow [MO_5V_O^{\bullet}] + [WO_6]^x \quad (5)$$

$$2[MO_6]' + [WO_6]^{\bullet\bullet} \longrightarrow 2[WO_6]^x + [WO_6]^x \quad (6)$$

Depolarization of $[MO_6]^x$ clusters:

$$[MO_5V_O^*].O_2 \longrightarrow [MO_5V_O^{\bullet}].O_2(ads) \quad (7)$$

$$[MO_5V_O^*]O_2 \longrightarrow [MO_5V_O^{\bullet\bullet}].O_2' \quad (8)$$

High $[V_O^{\bullet}]$ concentration adsorbs O_2 leading to $[MO_5V_O^{\bullet\bullet}]\cdot O_2'$ species.

Increasing tungsten concentration leads to $[MO_5V_O^{\bullet\bullet}]\cdot O_2'$ clusters. This species favour the creation of oxygen vacancies in $[TiO_6]$ or $[ZrO_6]$ sites, most of that being considered as complex vacancies in order-disorder structure. As a consequence, the oxygen vacancy-acceptor ion dipole may interact with polarization within a domain making its movement more difficult to switch.

XRD patterns of *BZT* and *BZTW* modified ceramics are shown in Fig. 4. Small traces of unreacted oxides such as TiO_2 and ZrO_2 are located at 2θ = 27 and 46 degree for the *BZT* phase. On the other hand, no secondary phases are evident in the *BZT1W* and *BZT2W* powders. This is a clear indication that the addition of tungsten has formed a stable solid solution in the *BZT* matrix lattice.

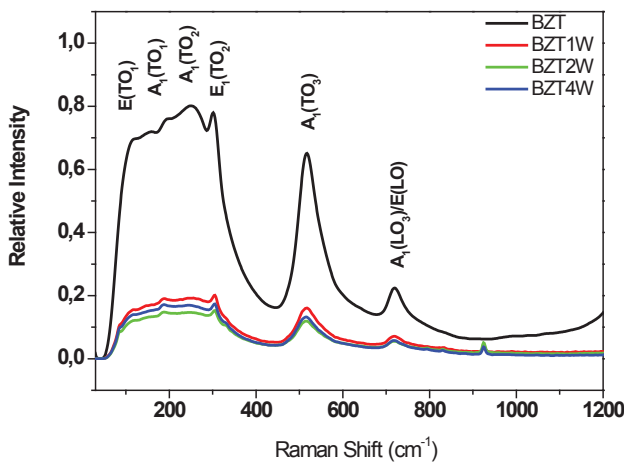

Figure 5. Room temperature depolarized Raman spectra for *BZT*, *BZT1W*, *BZT2W* and *BZT4W* powders prepared from mixed oxide method

As tungsten content increases, an intermediate phase of $BaWO_3$ has been obtained. Bragg reflection peaks are indicative of perovskite structure, mainly characterized by higher intense peak (*hkl*-110) at $2\theta = 31°$ and no apparent peak splitting is identified. Rietveld analysis is being evaluated and will be discussed in a future work.

Room temperature Raman spectra are displayed in Fig. 5. The evolution of Raman spectra in the tungsten substituted *BZT* ceramics shows some interesting changes. The order-disorder degree of the atomic structure at short range was noticed.

The spectrum shows the stretching mode of A1(TO1) and A1(TO3) at around 193 and 517 cm^{-1}. The E1(TO1) and E1(TO2) modes that have been associated with the tetragonal-cubic phase transition were observed at 116 and 301 cm^{-1}, whereas the A1(LO3) mode was found at 720 cm^{-1}, with zirconium (Zr) substituting on titanium (Ti) sites. As tungsten is incorporated in the *BZT* lattice, a Raman line at 925 cm^{-1} appears. Considering that tungsten substitutes the *B*-site of the lattice, as its content increases the relative intensity of bands reduces due to the distortion of octahedral sites. This results in diminished interstices in oxygen octahedron. Such observations could not be observed in the X-ray studies due to the different coherence length and time scale involved in the process.

Fig. 6 shows the temperature dependence of relative dielectric permittivity and dielectric losses measured at 10 KHz for selected *BZT* compositions. Substitution of W^{6+} in the *B*-site will lead to the distortion of the perovskite lattice leading to a reduction of phase transition temperature up to tungsten content of 2 wt.% and broadening of dielectric peak. Since the ionic radius of W^{6+} is smaller (0.62 Å) than that of Ti^{4+} = 0.68 Å on *B*-site, increasing its amount would lead to a reduced contribution of overall atomic polarization. The dielectric permittivity increases gradually with an increase in temperature up to the transition temperature (T_c), Curie point, and then decreases. The region around the dielectric peak is broadened due to a disorder in the cations arrangement in one or more crystallographic sites of the structure [16,17]. Large differences in the *B* valence results in a strong tendency for the material to disorder in one or more crystallographic sites leading to a microscopic heterogeneity in compounds with different Curie points [18]. According to Wu [17], the dielectric permittivity consists of contributions of ionic and atomic polarization only. Therefore, the increase of dielectric permittivity may be attributable to increased ionic polarization. Jin *et al.* [18] proposed that the phase transition is caused by instability of the BO_6 octahedra. The relatively larger ionic radius of the B ion enhances the thermal stability of the BO_6 octahedra, when compared to Ti or Zr [19]. This results in an increase of BO_6 volume octahedron and consequently decreasing its stability which results in a reduction of phase transition. Other factor can be the instability of the oxygen octahedron that involves the *B* cation lead-

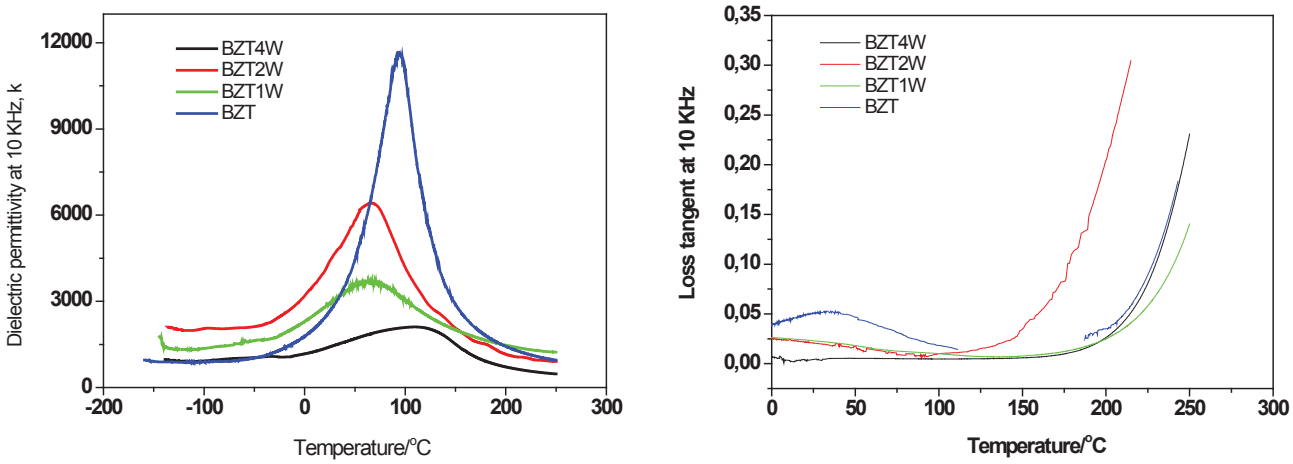

Figure 6. Temperature dependence of dielectric permittivity at 10 KHz for *BZT*, *BZT1W*, *BZT2W*, *BZT4W* ceramics prepared from mixed oxide method (a) and temperature dependence of loss tangent at 10 KHz for *BZT*, *BZT1W*, *BZT2W* and *BZT4W* ceramics prepared from mixed oxide method (b)

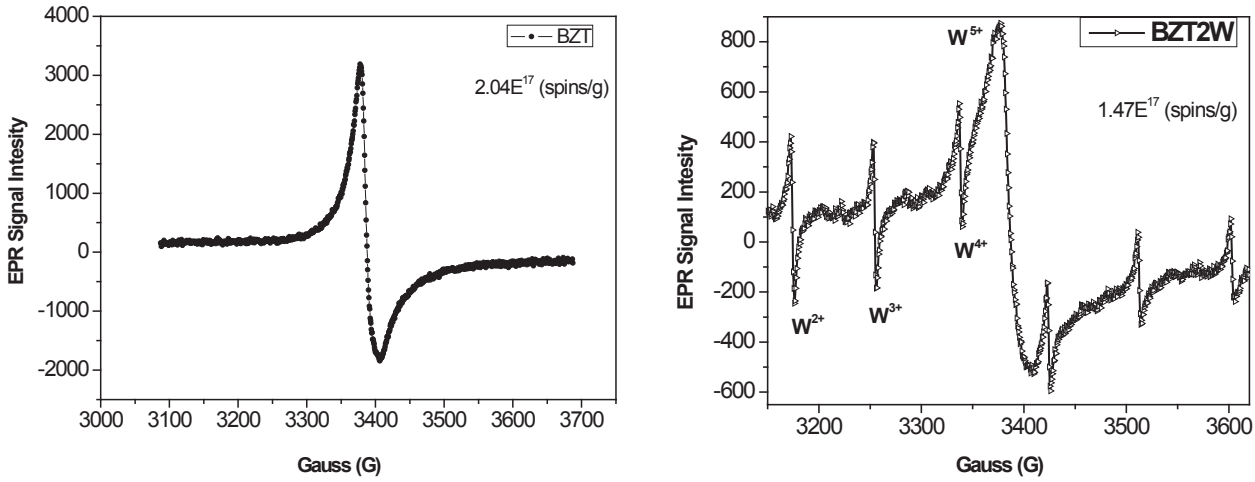

Figure 7. Electron paramagnetic resonance measurements for *BZT* and *BZT2W* powders

ing to a phase transition reduction. This involves structural inhomogeneity and existence of polar nanoregions. The interstices in oxygen octahedron will be diminished with the increase of metal vacancies in the *B*-site, and the c/a ratio will be lowered as well. Therefore, the dielectric polarization is depressed owing to the restraint of the *B*-site cations, and as a result the Curie point will lead to a diffuse phase transition. The dielectric permittivity is reduced with the increase in tungsten content leading to a typical relaxor behaviour. At lower temperatures, a small dependence of dielectric loss was observed while at elevated ones, there is a significant dependence on it. Also, a small peak just below T_c was evident in the *BZT*. It should be pointed out that this behaviour can be explained by the appearance of polar microregions in the samples. The dielectric relaxation peak can be attributed to the electron-relaxation-mode coupling mechanism in which carriers (or polarons, protons, and so on) are coupled with existing dielectric modes suggesting that the motion of carriers (or polaron hopping) is responsible for this behavior [20]. The formation of *B*-site vacancies has lead to an increase of dielectric loss at elevated temperatures, contrary to that observed in La^{3+} doped *PZT* ceramics [21]. Poor insulation resistance was maintained at high temperatures indicating that these ceramics can be used for low temperature capacitor applications. In addition, the dielectric loss was much lower than that of the undoped *BZT* reported in our previous work [22–24], which is attributed to the decrease in space charge density as tungsten was incorporated in the *BZT* lattice. Two main mechanisms can be considered for substituting W for Ti in the *BZT* lattice. The compensation mechanism for substituting a 6+ ion for a 4+ ion should reduce the oxygen vacancy concentration, leading to formation of Ba^{2+} vacancies. Another possibility is that the extra electrons become somewhat delocalized leading to some conductivity.

Room-temperature EPR spectra are shown in Fig. 7. EPR Hamiltonian parameters were used to perfectly reproduce the observed sequence of symmetrical peak pattern of the fine structure. Substitution of W^{6+} in the Ti site (Fig. 7b) causes a slight distortion in the spectra increasing disorder and symmetry changes in the *BZT* lattice (Fig. 7a). Charges were quantitatively determined and illustrated. BZT2W spectra shows hyperfine bands typical for materials with spin 5/2 which can be attributed to the ^{91}Zr presence as proposed by Abraham *et al.* [25]. Moreover, it suggests almost isotropic neighbourhood of the isolated Zr and Ti ions in the pattern. The obtained signal is typical for single ionized oxygen vacancies $V_O^{\bullet}$, as observed by Zhang *et al.* [26]. The hyperfine bands in the spectra correspond to the expected line broadening attributed to dipolar interactions of tungsten in the host, according to reaction of defects as discussed in literature [27]. Substitution of Ti^{4+} with W^{6+} causes distortion in the crystal structure changing lattice parameter. In this structure, $[TiO_5.Vo^x]c$ clusters are donor candidates and $[TiO_6]^xc$ are acceptors candidates. $[TiO_5.Vo^x]c$ have shown two paired electrons $\underline{\uparrow\downarrow}$, $[TiO_5.V_O^{\bullet}]c$ have shown one unpaired electron $\underline{\uparrow}$, while $[TiO_5.V_O^{\bullet\bullet}]c$ have shown no unpaired electrons. The source of hyperfine bands can be a result of interaction between an ion with unpaired electrons with species which present complex vacancies. This is supported by the high symmetry as inferred from Raman studies. The main differences in the spectra correspond to the expected line broadening attributed to dipolar interactions of tungsten in the host, according to equations 1–8.

IV. Conclusions

Undoped and tungsten doped $Ba(Ti_{1-x}Zr_x)O_3$ (*BZT*) ceramics were attained by the mixed oxide method. The maximum sintering temperature is reduced after tungsten addition due to generation of oxygen vacancies. The tungsten doped *BZT* powders consist of soft agglomerates which were completely broken during milling process and densified at lower temperatures. Tung-

sten addition leads to the distortion of the perovskite lattice leading to typical relaxor behaviour. Dielectric properties have been investigated and a maximum dielectric permittivity for the undoped *BZT* reached 11500 at a Curie temperature of 93°C. The dielectric permittivity is reduced and shifted to lower temperatures up to a tungsten content of 2 wt.%. Room-temperature EPR spectrum evidenced hyperfine bands resulting from interaction between species with unpaired electrons with species which present complex vacancies. The BZT2W (2 wt.% W doped BZT) ceramic showed a relaxor-like behaviour near phase transition which can be useful for low temperature capacitor applications.

Acknowledgments: The authors gratefully acknowledge the financial support of the Brazilian financing agencies FAPESP, CNPq and CAPES.

References

1. D. Hennings, A. Schnell, "Diffuse ferroelectric phase-transitions in $Ba(Ti_{1-y}Zr_y)O_3$ ceramics", *J. Am. Ceram. Soc.*, **65** (1982) 539–544.
2. D. Hennings, B. Schreinemacher, H. Schreinemacher, "High-permittivity dielectric ceramics with high endurance", *J. Eur. Ceram. Soc.*, **13** (1994) 81–88.
3. S.M. Neirman, "The Curie Point Temperature of $Ba(Ti_{1-x}Zr_x)O_3$ Solid Solution", *J. Mater. Sci.*, **23** (1988) 3973–3980.
4. M. McQuarrie, F.W. Behnke, "Structural and dielectric studies in the system $(Ba,Ca)(Ti,Zr)O_3$", *J. Am. Ceram. Soc.*, **37** (1954) 539–543.
5. R.C. Kell, N.J. Hellicar, "Structural transitions in barium titanate- zirconate transducer materials", *Acusticu.*, **6** (1956) 235–238.
6. T.N. Verbitshais, S.S. Zhdanov, Iu.N. Venevtsev, S.P. Solsviev, "Phenomenological theory of successive phase transitions in dielectric materials", *Sov. Phys. Crystallogr.*, **3** (1958) 182–185.
7. J. Ravez, A. Simon, "The crystal chemistry of the higher tungsten oxides", *J. Solid State Chem.*, **34** (1997) 1199–1203.
8. J. Ravez, A. Simon, "Raman spectroscopy and soft modes in the model ferroelastics", *Eur. Phys. J.: Appl. Phys.*, **11** (1997) 9–13.
9. R. Farhi, M. El Marssi, A. Simon, J. Ravez, "A Raman and dielectric study of ferroelectric $Ba(Ti_{1-x}Zr_x)O_3$ ceramics", *Eur. Phys. J. B.*, **9** (1999) 599–604.
10. Y. Zhi, A. Chen, J. Zhi, P.M. Vilarinho, J.L. Baptista, "Dielectric properties of $Ba(Ti_{1-x}Zr_x)O_3$ solid solutions", *J. Phys.*, **88** (2000) 410–414.
11. A. Carg, T.C. Goel, "Dielectric properties of NiZn ferrites by the precursor method", *Mater. Sci. Eng. B.*, **60** (1999) 156–160.
12. R. Shannigrahi, R.N.P. Choudhary, N. Acharya, "Electrohydrodynamic instability in 8CB (4'-n-octyl-4-cyanobiphenyl) liquid crystal", *Mater. Sci. Eng. B.*, **56** (1999) 31–35.
13. D. Bolten, U. Bouger, T. Schneller, M. Grossnam, O. Lose, R. Waser, "Reversible and irreversible processes in donor-doped $Pb(Zr,Ti)O_3$", *Appl. Phys. Lett.*, **77** (2000) 3830–3832.
14. S. Takahashi, "Effects of impurity doping in lead zirconate-titanate ceramics", *Ferroelectrics.*, **41** (1982) 277–290.
15. X.S. Wang, H. Ishiwara, "Polarization enhancement and coercive field reduction in W- and Mo-doped $Bi_{3.35}La_{0.75}Ti_3O_{12}$ thin films". *Appl. Phys. Lett.*, **82** (2003) 2479–2481.
16. M.E. Lines, A.M. Glasss, *Principles and applications of ferroelectrics and related materials*, Oxford University Press, Oxford 1977.
17. Y. Wu, S.J. Limmer, T.P. Chou, C. Nguyen, C. Guozhong, "Influence of tungsten doping on dielectric properties of strontium bismuth niobate ferroelectric ceramics", *J. Mater. Sci. Lett.*, **21** (2002) 947–949.
18. D. Jin, P. Hing, C.Q. Sun, "Intense and stable blue-light emission of $Pb(Zr_xTi_{1-x})O_3$", *Appl. Phys. Lett.*, **79** (2001) 1082–1084.
19. L. Wu, C. Wei, T. Wu, H. Liu, "Effects of dye loading", *J. Phys. C: Solid State Phys.*, **16** (1983) 2803–2806.
20. Y.H. Xu, *Ferroelectric Materials and their Applications*, Elsevier Science Publishers Amsterdam, 1991.
21. L. Wu, C. Wei, T. Wu, H. Liu, "Dielectric properties of modified PZT ceramics", *J. Phys. C: Solid State Phys.*, **16** (1983) 2803–2806.
22. F. Moura, A.Z. Simões, E.C. Aguiar, I.C. Nogueira, M.A. Zaghete, J.A. Varela, E. Longo. "Dielectric investigations of vanadium modified barium titanate zirconate ceramics obtained from mixed oxide method", *J. Alloys Compd.*, **479** (2009). 280–283.
23. F. Moura, A.Z. Simões, C.A. Paskocimas, M.A. Zaghete, E. Longo. J.A. Varela, "Temperature Dependence of Electrical Properties of BZT:2V ceramics", *Mater. Chem. Phys.*, in press, 2010.
24. L.G.A. Marques, L.S. Cavalcante, A.Z. Simões, F.M. Pontes, L.S. Santos-Junior, M.R.M.C. Santos, I.L.V. Rosa, J.A. Varela, E. Longo, "Temperature dependence of dielectric properties for $Ba(Zr_{0.25}Ti_{0.75})O_3$ thin films obtained from the soft chemical method", *Mater. Chem. Phys.*, **105** (2007) 293–297.
25. M.M. Abraham, L.A. Boatner, M.A. Aronson, "EPR observations of trivalent titanium in orthophosphate single crystals", *J. Chem. Phys.*, **85** (1986) 1–6.
26. M. Zhang, Z. Jin, J. Zhang, X. Gou, J. Yang, X. Wang, Z. Zhang, "Effect of annealing temperature on morphology, structure and photocatalytic behavior of nanotubed $H_2Ti_2O_4(OH)_2$", *J. Mol. Catal. A: Chem.*, **217** (2004) 203–210.
27. R. Shannigrahi, R.N.P. Choudhary, N. Acharya, "Phase transition in $Ba_5RTi_3Nb_7O_{30}$ (R = Dy, Sm) ferroelectric ceramics", *Mater. Sci. Eng.*, B **56** (1999) 27–31.